

IMAGE PROCESSING

PACS numbers: 07.60.Fs; 42.25.Lc; 87.19.xj
DOI: 10.1070/QE2012v042n08ABEH014825

Spatial-frequency Fourier polarimetry of the complex degree of mutual anisotropy of linear and circular birefringence in the diagnostics of oncological changes in morphological structure of biological tissues

Yu.A. Ushenko, M.P. Gorskii, A.V. Dubolazov, A.V. Motrich, V.A. Ushenko, M.I. Sidor

Abstract. **Theory of polarisation-correlation analysis of laser images of histological sections of biopsy material from cervix tissue based on spatial frequency selection of linear and circular birefringence mechanisms is formulated. Comparative results of measuring the coordinate distributions of the complex degree of mutual anisotropy (CDMA), produced by fibrillar networks formed by myosin and collagen fibres of cervix tissue in different pathological conditions, namely, pre-cancer (dysplasia) and cancer (adenocarcinoma), are presented. The values and variation ranges of statistical (moments of the first–fourth order), correlation (excess-autocorrelation functions), and fractal (slopes of approximating curves and dispersion of extrema of logarithmic dependences of power spectra) parameters of the CDMA coordinate distributions are studied. Objective criteria for pathology diagnostics and differentiation of its severity degree are determined.**

Keywords: *laser, polarisation, Fourier filtration, correlation, biological tissue, birefringence, crystal, statistical moment, fractal.*

1. Introduction

Optical methods of biological tissues study may be divided into the following constitutive groups.

(i) Spectrophotometric methods, which are based on the analysis of spatial or temporal changes of the laser radiation intensity, scattered by biological tissues [1, 2].

(ii) Polarisation methods, based on the use of the complex amplitude coherence matrix and on the analysis of the polarisation degree as a factor of correlation between the complex orthogonal components of electromagnetic oscillations at one of the points of the scattered laser radiation field [3–12].

(iii) Correlation methods based on the analysis of the degree of correlation between the parallel polarisation components of the light oscillations at different points of the object field [13–20].

The new 'two-point' polarisation-correlation approach to the study of the fields, scattered by biological tissues, became a generalisation of the abovementioned directions of optical biotissue diagnostics. This approach, proposed and developed in a series of theoretical [21–24] and applied [25–28] research works, is based on the use of new parameters for description of interrelations between the coordinate structures of optically anisotropic protein networks {complex degree of mutual anisotropy (CDMA) [25, 26]} and their laser images {complex degree of mutual polarisation (CDMP) [27]}. At the same time, the theoretical background of the polarisation correlometry methods, based on the linear birefringence approximation, needs further development and improvement. First it is necessary to account for alternative transformation mechanisms of laser radiation parameters, namely, the optical activity or circular birefringence, dichroism, etc. [9, 10, 17–19]. Therefore, further progress in the optical studies of the properties of optically anisotropic protein networks of biological tissues may be associated with the development of novel method of diagnostics and selection of the linear and circular birefringence parameters aimed at revealing and differentiation of the degree of severity of pathological changes.

The aim of our work is to develop a method for measuring CDMA using the spatial frequency filtering of manifestations of linear and circular birefringence in fibrillar protein networks for diagnostics and differentiation of pathological (benign and malignant) changes in tissues of a reproductive female organ, the cervix.

2. Theory of the method

The authors of [25, 26] first proposed a new parameter (CDMA) for characterisation of the degree of alignment of optical axes and birefringence at different points (r_1, r_2) of a fibrillar network of biotissue protein crystals:

$$W(r_1,r_2) = \{[d_{11}(r_1)\, d_{11}(r_2) - d_{12}(r_1)\, d_{12}(r_2)] + [d_{21}(r_1)\, d_{21}(r_2) - d_{22}(r_1)\, d_{22}(r_2)]\}^2 / [I(r_1)\, I(r_2)], \quad (1)$$

where d_{ik} are the elements of the Jones matrix [29] of the optically anisotropic fibril linear birefringence at two points with the coordinates (r_1, r_2).

In our work we consider the possibility of further development of this approach for a more general case of multilayer biological tissue (cervix) with the generalised optical anisotropy (linear and circular birefringence) taken into account.

The analysis of the processes of amplitude-phase modulation of laser radiation by such object is based on the following model conceptions [30–36].

(i) The cervix consists of two optically anisotropic layers of muscle (myometrium) and connective (endometrium) tissues.

Yu.A. Ushenko, M.P. Gorskii, A.V. Dubolazov, A.V. Motrich, V.A. Ushenko, M.I. Sidor Yuriy Fedkovich Chernivtsi National University, ul. Kotsubinskogo 2, 58012 Chernivtsi, Ukraine; e-mail: ushenko@itf.cv.ua

Received 11 February 2012; revision received 27 April 2012
Kvantovaya Elektronika **42** (8) 727–732 (2012)
Translated by V.L. Derbov

(ii) The optically anisotropic network of myometrium consists of large-scale (transverse dimension $l \sim 50-200$ μm) filament-like (length $L \gg l$) myosin fibrils with presumably linear birefringence (at the expense of ordered packing that determines the directions of the optical axes of partial biological crystals).

(iii) The optically anisotropic component of endometrium is formed by collagen fibres with disordered directions of optical axes ($l \sim 5-25$ μm, $L \approx l$) with presumably circular birefringence.

(iv) Polarisation properties of the point of fibrillar network are characterised by the generalised matrix of optical anisotropy

$$\{D\} = \{Q\}\{A\}, \tag{2}$$

where

$$\{Q\} = \begin{Vmatrix} \sin^2\rho + \cos^2\rho\exp(-i\delta) & \sin\rho\cos\rho[1-\exp(-i\delta)] \\ \sin\rho\cos\rho[1-\exp(-i\delta)] & \cos^2\rho + \sin^2\rho\exp(-i\delta) \end{Vmatrix} \tag{3}$$

is the Jones matrix for linear birefringence;

$$\{A\} = \begin{Vmatrix} \cos\theta & -\sin\theta \\ \sin\theta & \cos\theta \end{Vmatrix} \tag{4}$$

is the Jones matrix of circular birefringence, or optical activity. Here ρ is the angle with the direction of the optical axis; $\delta = (2\pi/\lambda)\Delta n l$ is the phase shift between the orthogonal components of the laser radiation amplitude with the wavelength λ that passed the geometric path l through the biological crystal with the difference of linear refractive indices of ordinary and extraordinary waves (birefringence index) Δn; θ is the rotation angle of the laser wave polarisation plane, caused by circular birefringence.

Taking the small value of the birefringence index ($\Delta n \sim 10^{-3}$) and the insignificant transverse dimensions of protein fibrils into account, without loss of the analysis completeness, we restrict ourselves to the weak anisotropy approximation, in which the magnitude and fluctuations of the parameters δ and θ are sufficiently small. In this situation one can assume that

$$\cos\begin{pmatrix}\delta\\ \theta\end{pmatrix} \approx 1, \quad \sin\begin{pmatrix}\delta\\ \theta\end{pmatrix} \approx \begin{pmatrix}\delta\\ \theta\end{pmatrix}$$

and rewrite the matrix operators (3), (4) in the following way:

$$\{Q\} = \begin{Vmatrix} \sin^2\rho + \cos^2\rho(1-i\delta) & i\delta\sin\rho\cos\rho \\ i\delta\sin\rho\cos\rho & \cos^2\rho + \sin^2\rho\exp(1-i\delta) \end{Vmatrix}, \tag{5}$$

$$\{A\} = \begin{Vmatrix} 1 & -\theta \\ \theta & 1 \end{Vmatrix}. \tag{6}$$

Let us clarify the capabilities of space frequency filtering for separation of CDMA coordinate distributions, produced by different components of the probed cervix layer with linear and circular birefringence. For this aim let us consider the process of transformation ($E_0 \to (\rho,\delta,\theta) \to E$) of a plane-polarised laser wave having the azimuthal angle 0^0 and described by the Jones vector

$$E_0 = \begin{bmatrix} E_{0x}\exp(-i\varphi_{0x}) \\ E_{0y}\exp(-i\varphi_{0y}) \end{bmatrix} \longrightarrow E_0(0^0) = \begin{pmatrix}1\\0\end{pmatrix}.$$

The Jones vector

$$E = \begin{bmatrix} E_x\exp(-i\varphi_x) \\ E_y\exp(-i\varphi_y) \end{bmatrix}$$

of the transformed radiation is determined by the following matrix equation:

$$E = \{D\}E_0. \tag{7}$$

With the relations (5), (6) taken into account, the orthogonal components of the amplitude of the Jones vector E of the transformed laser beam are expressed as

$$\begin{aligned} E_x(0^0) &= 1 - i\delta\cos\rho(\cos\rho + \theta\sin\rho), \\ E_y(0^0) &= \theta - i\delta\sin\rho(\cos\rho + \theta\sin\rho). \end{aligned} \tag{8}$$

From a medical point of view an urgent problem is the 'optical selection' of polarisation manifestations of linear (ρ,δ) and circular (θ) birefringence by the network of protein fibrils of the cervix myometrium and endometrium layers for diagnostics of the occurrence and differentiation of the pathological process severity degree. The problem is that at early stages the pathological changes are localised in the endometrium surface layer and are accompanied by the growth of the collagens concentration ($\theta\uparrow$) in the relevant fibrillar network. A more developed pathological condition is manifested by the growth of the myosin concentration ($\delta\uparrow$) and malignant neoplasm growth direction formation in the myometrium layer [37]. Traditional histological diagnostics and differentiation of such pathologies is rather labour-consuming, require much time and often appear ambiguous [38]. We propose to base optical selection of such states on the method of spatial frequency filtering of the laser radiation field in the Fourier plane. In this plane the distributions of complex amplitudes are produced, which are mathematically defined by the direct Fourier transform of Eqns (8):

$$U_x\left(\frac{X}{\lambda f},\frac{Y}{\lambda f}\right) \equiv U_x(v,\mu) = \frac{1}{i\lambda f}\iint_{-\infty}^{\infty}\exp[-i2\pi(xv+y\mu)]dxdy$$

$$-\frac{1}{\lambda f}\iint_{-\infty}^{\infty}\delta\cos\rho(\cos\rho+\theta\sin\rho)\exp[-i2\pi(xv+y\mu)]dxdy, \tag{9}$$

$$U_y\left(\frac{X}{\lambda f},\frac{Y}{\lambda f}\right) \equiv U_y(v,\mu) = \frac{1}{i\lambda f}\iint_{-\infty}^{\infty}\theta\exp[-i2\pi(xv+y\mu)]dxdy$$

$$-\frac{1}{\lambda f}\iint_{-\infty}^{\infty}\delta\cos\rho(\cos\rho+\theta\sin\rho)\exp[-i2\pi(xv+y\mu)]dxdy. \tag{10}$$

Here $U_x(v,\mu)$, $U_y(v,\mu)$ are the Fourier transforms of the distributions $E_x(\rho,\delta,\theta)$ and $E_y(\rho,\delta,\theta)$ in the focal (f) plane of the objective lens; $v = X/(\lambda f)$, $\mu = Y/(\lambda f)$ are the normalised spatial frequencies. From (9) and (10) it follows that the spatial frequency structure of the distributions $U_x(v,\mu)$, $U_y(v,\mu)$ is determined by the sum of harmonics $\exp[-i2\pi(xv + y\mu)]$ with the periods of spatial modulation $L(v,\mu) = \lambda f/(v^2+\mu^2)^{1/2}$. It is easy to see the fibrillar stroma networks and parenchyma epithelial plates being different in geometrical dimensions dem-

onstrate the Fourier transforms of the distributions $E_{x,y}(\rho,\delta,\theta)$ (8), modulated at different frequencies. Therefore, if in the central part of the Fourier plane a transparent $[R(\Delta v,\Delta\mu)]$ or opaque $[R^{-1}(\Delta v,\Delta\mu)]$ vignetter is placed, i.e.,

$$\hat{U}(\rho,\delta,v,\mu) = R(\Delta v,\Delta\mu)\,U(v,\mu),$$

$$\hat{U}(\theta,v,\mu) = R^{-1}(\Delta v,\Delta\mu)\,U(v,\mu),$$

then using an inverse Fourier transform one can reconstruct the low- and high-frequency components

$$\hat{U}_x(R,v,\mu) \sim \frac{1}{\lambda f}\iint_{-\infty}^{\infty}\delta\cos^2\rho\exp[-\mathrm{i}2\pi(x\Delta v + y\Delta\mu)]\mathrm{d}x\mathrm{d}y,$$
$$\hat{U}_y(R,v,\mu) \sim \frac{1}{\lambda f}\iint_{-\infty}^{\infty}\delta\sin^2\rho\exp[-\mathrm{i}2\pi(x\Delta v + y\Delta\mu)]\mathrm{d}x\mathrm{d}y, \quad (11)$$

$$\hat{U}_x(R^{-1},v,\mu) \sim \frac{1}{\lambda f}\iint_{-\infty}^{\infty}\theta\sin\rho\cos\rho \times\exp[-\mathrm{i}2\pi(x\Delta v + y\Delta\mu)]\mathrm{d}x\mathrm{d}y,$$
$$\hat{U}_y(R^{-1},v,\mu) = \frac{1}{\mathrm{i}\lambda f}\iint_{-\infty}^{\infty}\theta(1+\sin\rho) \times\exp[-\mathrm{i}2\pi(x\Delta v + y\Delta\mu)]\mathrm{d}x\mathrm{d}y. \quad (12)$$

The transformations (11) and (12) allow determination of coordinate distributions of the Jones matrix elements for linear $[q_{ik}(\rho,\delta)]$ and circular $[a_{ik}(\theta)]$ birefringence in accordance with the classical technique [28]. Taking the obtained data and the basic relation (1) into account, we find the analytic expressions of the CDMA parameter for different types of optically anisotropic components of the cervix:

$$W_{\rho,\delta}(r_1,r_2) \sim [q_{11}(r_1)\,q_{11}(r_2) + q_{22}(r_1)\,q_{22}(r_2) + 0.5\sin2\rho(r_1)\sin2\rho(r_2)\delta(r_1)\,\delta(r_2)]^2/[I(r_1)\,I(r_2)], \quad (13)$$

$$W_\theta(r_1,r_2) \sim \frac{[1-\theta(r_1)\theta(r_2)]^2}{I(r_1)I(r_2)}. \quad (14)$$

3. Optical implementation of spatial frequency filtering of the CDMA coordinate distributions for protein networks of the cervix tissue layers

As objects of study we took two groups of optically thin (attenuation coefficient $\tau \approx 0.087-0.093$) histological sections of the cervical tissue, prepared by the standard technique including the freezing microtome from two groups of patients with the following diagnoses: pre-cancer condition (dysplasia) – 21 samples (group 1), cancer – 19 samples (group 2).

The experimental investigation of coordinate distributions of the CDMA was performed using the classical polarimeter [25–27], the main units and elements of which are presented in Fig. 1.

A polarised light source [quarter-wave plates (*3*), (*5*) and polariser (*4*)] sequentially produced a set of probing linearly polarised laser beams with the azimuthal angles $\alpha_0 = 0$, 45°, 90° and a circular right-polarised wave (⊗).

The histologic sections (*6*) of biopsy material from cervix were placed in the focal plane of the polarisation microscopic objective (*7*) (numerical aperture 0.1, focal length 300 mm, magnification 4×). In the back focal plane (Fourier plane) a vignetter $F(u,v)$ was placed, the dimensions of which varied from 10 to 300 pixels; in this case the spatial frequency filtering of the boundary area of the histological section was implemented. Using the polarisation microscopic objective (*8*), placed at the focal length distance from the frequency plane of the microscopic objective (*7*), the inverse Fourier transform of the polarisation-filtered [quarter-wave plate (*9*) and polariser (*10*)] laser radiation field was implemented. For each polarisation type of the probing beam ($i \equiv 0$, 90°, 45°, ⊗) using the polarisation analyser the linear ($j \equiv 0$, 90°, 45°, 135°) and circular (right and left) polarisation filtering was provided. By means of the digital camera (*11*) the set of six coordinate intensity distributions $[I^{(i)}_{(j)})\ (m\times n)]$ of such a field was measured. Using the obtained data the coordinate distributions of the Jones matrix elements [29] were calculated, which characterised the properties of various birefringent structures of cervical stroma $[q_{ik}\ (m\times n)]$ and parenchyma $[a_{ik}\ (m\times n)]$. The value of CDMA $W(r_1, r_2 = r_1 + \Delta r)$ for two points $(r_1, r_2 + \Delta r)$ separated by the distance Δr in the plane of histological sections (*6*) was calculated using the relations (8) and (9). The coordinate distributions of the parameters $W_{\rho,\delta}(r_1,r_2)$ and

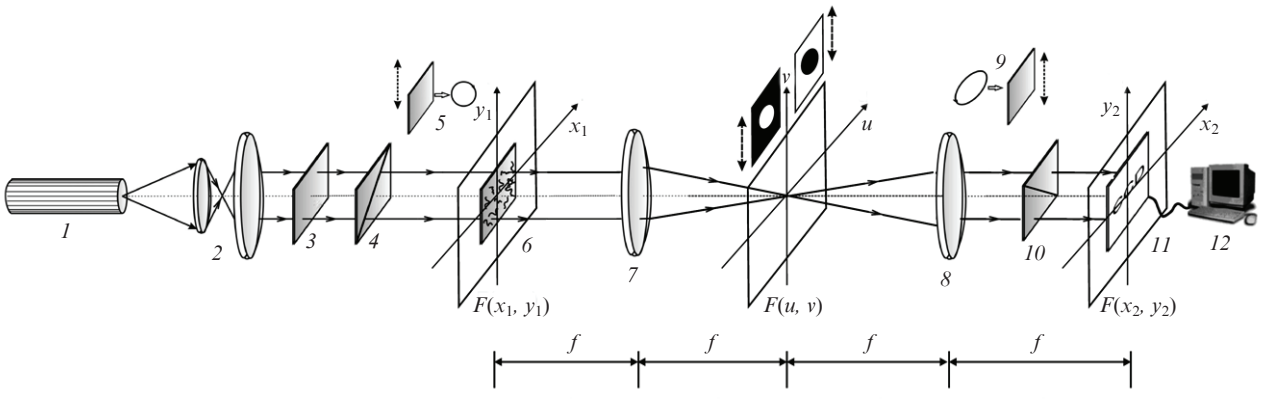

Figure 1. Optical scheme of Fourier polarimeter: (*1*) He–Ne laser; (*2*) collimator; (*3*) stationary quarter-wave plate; (*5*, *9*) rotary quarter-wave plates, (*4*, *10*) polariser and analyser; (*6*) object of study; (*7*, *8*) polarisation microscope objectives; (*11*) CCD-camera; (*12*) computer [$F(x_1,y_1)$ is the object plane, $F(u,v)$ is the Fourier plane with apertures, $F(x_2,y_2)$ is the plane of reconstructed (filtered) image].

$W_\theta(r_1, r_2)$ were determined by scanning the arrays q_{ik} $(m \times n)$ and a_{ik} $(m \times n)$ with the step $\Delta r = 1$ pixel in two mutually perpendicular directions ($x = 1 \div m$, $y = 1 \div n$).

For quantitative estimation of the distributions

$$q = \begin{cases} W_{\rho,\delta}(m \times n) \\ W_\theta(m \times n) \end{cases} \tag{15}$$

we used the following types of analysis: the statistical one (the statistical moments from first to fourth order $Z^W_{j=1,2,3,4}$ [6]), the correlation one (the 'correlation moments' Q^W_2 and Q^W_4 that determine the variance and the kurtosis of the autocorrelation function [8, 20]), and the fractal one {the slope of $V(\eta)$ and the dispersion D^W of the logarithmic dependences of power spectrum [11, 30, 32, 33]}.

4. Experimental results and discussion

At the first stage by means of direct polarimetry of laser images the coordinate distributions of CDMA [Eqn (1)] of the fibrillar network of cervix tissue samples were determined. The dependences, presented in Fig. 2, illustrate the statistical (c, d), correlation (e, g), and self-similar (f, h) structures of such distributions, found for histological sections of biopsy material with both types of pathology.

Comparative analysis of histograms (c, d), autocorrelation functions (e, g), and logarithmic dependences of power spectra (f, h) of CDMA distributions for polycrystalline networks (a, b) of histological sections of the cervix biopsy material did not reveal essential difference between the two types of pathology. This fact may be due to the superposition [Eqns (2), (7), (8)] of manifestations of linear and circular anisotropy of myosin and collagen fibrils of cervix myometrium and endometrium layers, which causes likeness of the statistical, correlation, and self-similar distribution structures of the CDMA distributions in the cases of dysplasia and cancer.

The dependences shown in Figs 3 and 4 illustrate the diagnostic potential for differentiation of the cervix tissue samples of both groups with the use of spatial frequency filtering in the Fourier plane [Eqns (9)–(12)].

Aimed at determining the optimal conditions to distinguish between the manifestations of linear [Eqns (3), (5)] and circular [Eqns (4), (6)] birefringence of myometrium and endometrium layers, the dimensions of the vignetter were varied within 10–200 μm. The optimal size was $R = 50$ μm, $R^{-1} = 30$ μm, for which the set of statistical moments from first to fourth order, characterising the CDMA distributions, takes the extremal values.

Comparative analysis of the collection of parameters characterising spatially and frequency filtered coordinate distributions $W_{\rho,\delta}(m \times n)$ of the large-scale network of myosin fibrils of the myometrium layer revealed certain difference between them. Namely, the histograms of CDMA distribution for a histological section of oncologically changed cervix tissue are characterised by asymmetric structure with a sharp peak of the principal extremum (Fig. 3f), in comparison with the analogous distribution, found for a tissue sample under the dysplasia condition (Fig. 3b). The revealed peculiarity, in our opinion, is related to the more ordered directions of the optical axes in the myosin network fibrillar structure (directions of malignant tumour growth) as compared with the case of myometrium dysplasia. Optically such geometrical construction ($\rho^* \leftrightarrow N_{\max}$) manifests itself in the formation of preferable, most probable values of CDMA $W_{\rho,\delta}(m \times n)$ [Eqns (3), (5), (13)], the ensemble of which is responsible for the principal extremum formation.

The autocorrelation functions for the CDMA distributions of fibrillar myosin networks in both samples decrease smoothly and monotonically (Figs 3c, g). This fact indicates coordinate-uniform structure of corresponding distributions $W_{\rho,\delta}(m \times n)$, produced by the mechanisms of interaction of laser radiation with the ensemble of linearly birefringent myosin fibrils. Besides that, we revealed the self-similar construction of such distributions: the logarithmic dependences of the power spectra $\lg J(W_{\rho,\delta}) - \lg d^{-1}$ are characterised by the same slope practically in the whole range 2–1000 μm of the geometrical dimensions variation (Figs 3d, h).

Thus, the main indication of cervix tissue oncological changes is the formation of spatially determined directions of

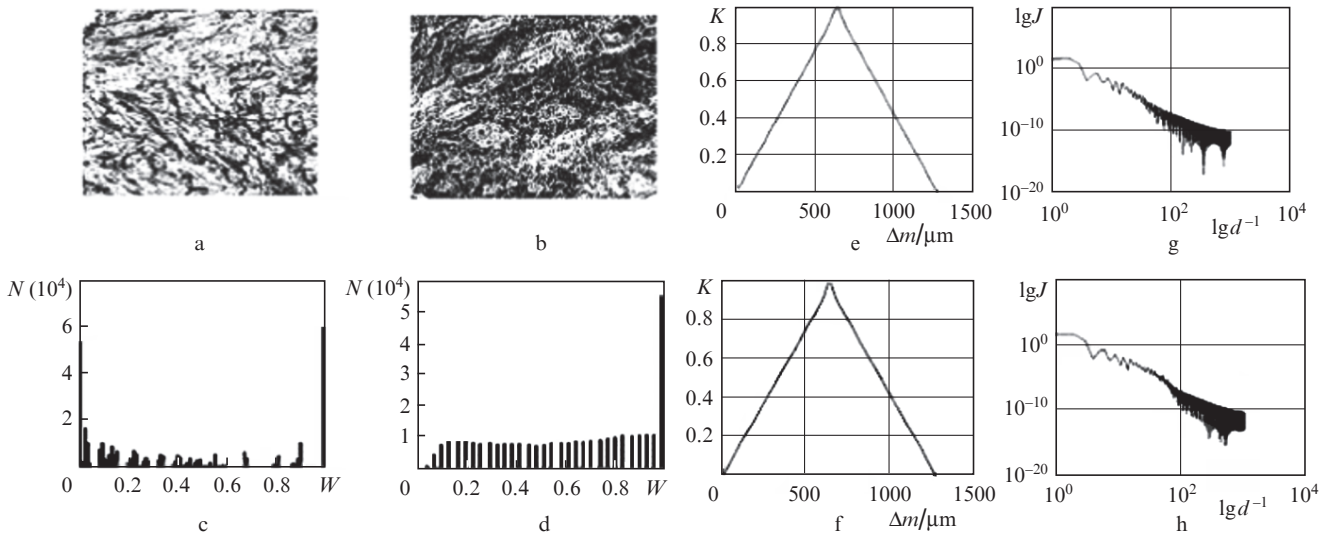

Figure 2. Coordinate patterns (a, b), histograms (c, d), autocorrelation functions (e, g), and logarithmic dependences of power spectra (f, h) of CDMA distributions of histological sections of cervix biopsy material from the patients of group 1 (a, c, e, f) and group 2 (b, d, g, h).

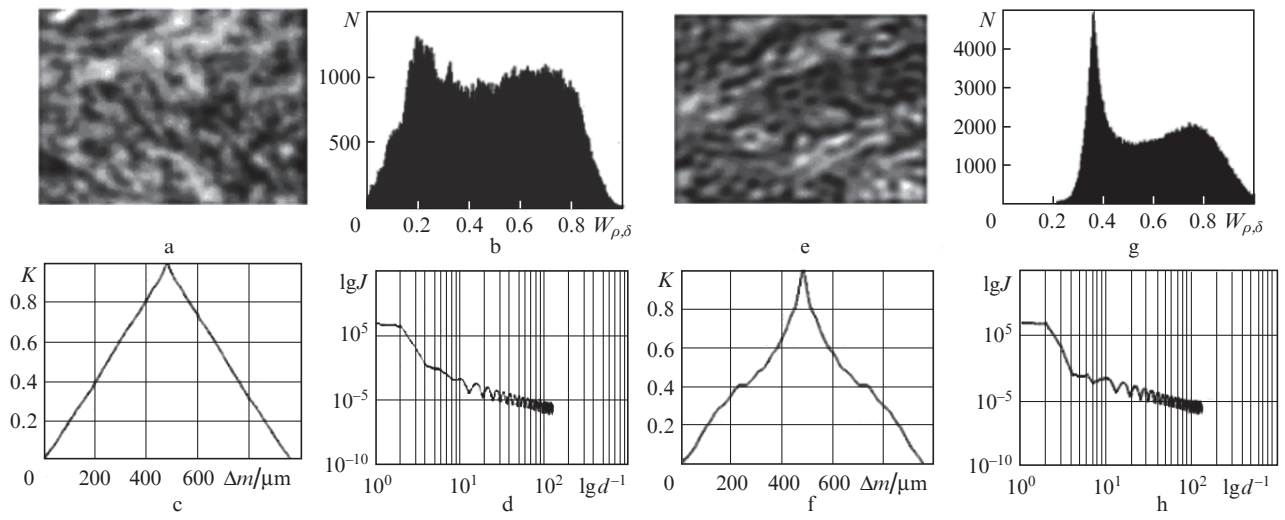

Figure 3. Coordinate patterns (a, e), histograms (b, f), autocorrelation functions (c, g), and logarithmic dependences of power spectra (d, h) of CDMA distributions of linear birefringence of histological sections of cervix tissue from the patients of group 1 (a–d) and group 2 (e–h).

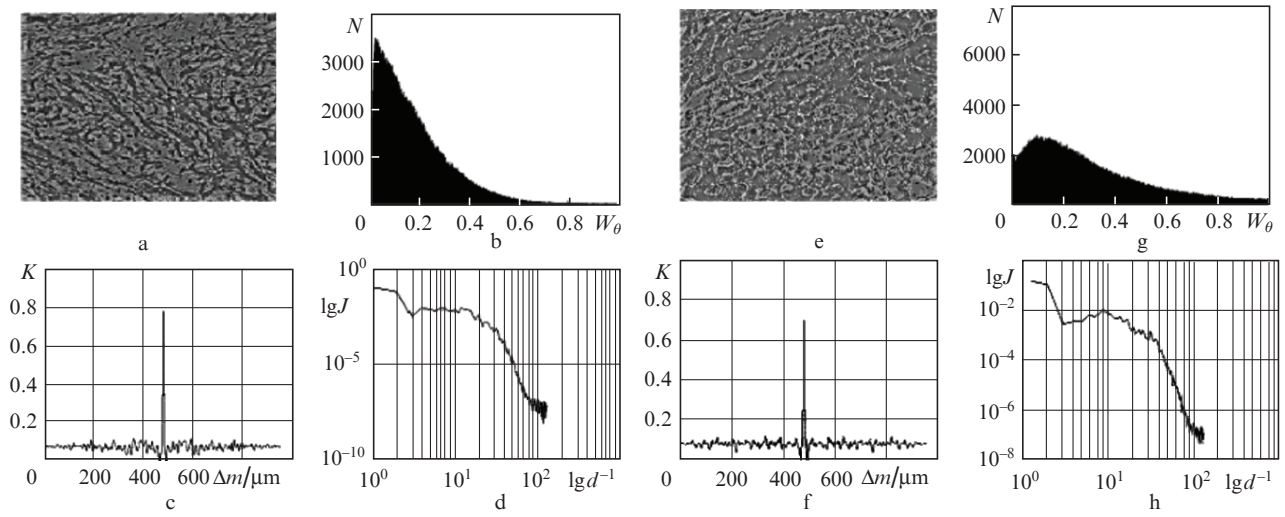

Figure 4. Coordinate patterns (a, e), histograms (b, f), autocorrelation functions (c, g), and logarithmic dependences of power spectra (d, h) of CDMA distributions of circular birefringence of histological sections of cervix tissue from the patients of group 1 (a–d) and group 2 (e–h).

the myosin fibrils growth [38] and related transformation of the histogram of CDMA distribution $W_{\rho,\delta}(m \times n)$.

A different situation is observed in the case of combined (statistical, correlation, and fractal) analysis of spatially and frequency filtered coordinate distributions of CDMA for small-scale optically active collagen networks of the endometrium layer (Fig. 4).

The comparison of the results (Figs 4a and e) revealed the following indications of the oncological condition of the cervix tissue.

(i) Substantial widening of the range in which the CDMA $W_\theta(m \times n)$ values vary for the fibrillar network of the endometrium layer (Figs 4b and f) due to the increase of the optically active collagen concentration.

(ii) 'Pathological' growth of the number of chaotically oriented fibrils, leading to a more homogeneous coordinate distribution $W_\theta(m \times n)$, which manifests itself in the increase in the half-width of the corresponding autocorrelation dependence $K(\Delta m)$ (Figs 4c and g).

(iii) Restructuring of the collagen optically-anisotropic network manifests itself in widening of the range of geometrical dimensions of local fibrils, which is accompanied by the increase in the dispersion of the extrema distribution of the dependences $\lg J(W_{\rho,\delta}) - \lg d^{-1}$ of the CDMA W_θ power spectrum, determined by the dimensional parameters of the collagen fibrils (Figs 4d and h).

Quantitatively, the difference between the coordinate distributions of CDMA parameters of linear [$W_{\rho,\delta}$ (13)] and circular [W_θ, (14)] birefringence of fibrillar networks of cervix myometrium and endometrium layers is illustrated by the mean values of the statistical, correlation and fractal parameters and their standard deviations within both groups (Table 1).

Comparative analysis of the results of spatial frequency Fourier polarimetry of the coordinate distributions of CDMA in fibrillar networks of the cervix tissue layers in different pathological condition revealed the following diagnostically efficient parameters (set off in boldface).

Table 1. Parameters of the statistical, correlation and self-similar structure of CDMA coordinate distributions for protein networks of cervix tissue.

Parameters	$W_{\rho,\delta}(m\times n)$		$W_{\theta}(m\times n)$	
	Dysplasia	Cancer	Dysplasia	Cancer
Z_1	0.49 ± 0.06	0.41 ± 0.07	$\mathbf{0.05\pm0.01}$	$\mathbf{0.18\pm0.02}$
Z_2	$\mathbf{0.34\pm0.05}$	$\mathbf{0.18\pm0.03}$	$\mathbf{0.14\pm0.02}$	$\mathbf{0.29\pm0.04}$
Z_3	$\mathbf{0.73\pm0.1}$	$\mathbf{2.2\pm0.4}$	$\mathbf{2.1\pm0.4}$	$\mathbf{1.03\pm0.1}$
Z_4	$\mathbf{0.89\pm0.02}$	$\mathbf{3.1\pm0.5}$	$\mathbf{1.7\pm0.2}$	$\mathbf{0.56\pm0.08}$
Ω_2	0.24 ± 0.04	0.21 ± 0.04	$\mathbf{0.04\pm0.01}$	$\mathbf{0.11\pm0.01}$
Ω_4	0.14 ± 0.02	0.18 ± 0.03	$\mathbf{4.5\pm0.7}$	$\mathbf{2.1\pm0.3}$
$V(\eta)$	Fractal	Fractal	Random	Random
D	0.32 ± 0.05	0.29 ± 0.04	$\mathbf{0.11\pm0.02}$	$\mathbf{0.19\pm0.02}$

1. Statistical moments of the second and fourth order that characterise the distributions $W_{\rho,\delta}(m\times n)$ for linearly birefringent fibrils – the difference amounts to 2–3 times.

2. Complete set of statistical moments of CDMA for the polycrystalline network with circular birefringence – the differences amount to 2–3 times.

3. Correlation moments of the second and fourth order of autocorrelation functions of distributions $W_{\theta}(m\times n)$ – the difference amounts to 2.2–3 times.

4. Variance of logarithmic dependences of the power spectra for the distributions $W_{\theta}(m\times n)$ – the difference reaches 2 times.

5. Conclusions

The method for determining the CDMA coordinate distributions of the cervix tissue with subsequent spatial frequency filtering of manifestations of linear and circular birefringence is proposed and analytically justified.

Comparative studies of the efficiency of use of the developed CDMA spatial frequency Fourier polarimetry methods for diagnostics of pathological condition of the cervix tissue and differentiation of the degree of its severity are performed.

The criteria for differentiation of cervical dysplasia and cancer on the base of the statistical (statistical moments of first–fourth order), correlation (second and fourth moments of autocorrelation function), and fractal (variance and slope of approximating curves log – log of the power spectrum dependences) analysis of the spatially and frequency filtered CDMA distributions of protein networks with linear and circular birefringence are established.

References

1. Tuchin V.V. *Usp. Fiz. Nauk*, **167**, 517 (1997) [*Phys.-Usp*., **40**, 495 (1997)].
2. Wang X., Yao G., Wang L.-H. *Appl. Opt*., **41**, 792 (2002).
3. Wang X., Wang L.-H. *J. Biomed. Opt*., **7**, 279 (2002).
4. Wang X., Wang L.-H., Sun C.-W., Yang C.C. *J. Biomed. Opt*., **8**, 608 (2003).
5. Seteikin A.Yu. *Izv. Vyssh. Uchebn. Zaved., Ser. Fiz*., **3**, 53 (2005) [*Russ. Phys. J*., **48** (3), 280 (2005)].
6. Numan O.K., Moiysuk T.G. *Adv. Opt. Technol*., **2010**, 423145 (2010).
7. Angelsky O.V., Tomka Yu.Ya., Ushenko A.G., Ushenko Ye.G., Ushenko Yu.A. *J. Phys. D: Appl. Phys*., **38**, 4227 (2005).
8. Angelsky O.V., Ushenko A.G., Ushenko Yu.A., Ushenko Ye.G., Tomka Yu.Ya., Pishak V.P. *J. Biomed. Opt*., **10**, 064025 (2005).
9. Guminetskiy S.H., Ushenko A.G., Polyanskiy I.P., Motrych A.V., Grynchuk F.V. *Proc. SPIE Int. Soc. Opt. Eng*., **7008**, 700827 (2008).
10. Yermolenko S., Ushenko A., Ivashko P., Goudail F., Gruia I., et al. *Proc. SPIE Int. Soc. Opt. Eng.*, **7388**, 73881D (2008).
11. Ushenko A., Yermolenko S., Prydij A., Guminetsky S., Gruia I., Toma O., Vladychenko K. *Proc. SPIE Int. Soc. Opt. Eng.*, **7008**, 70082C (2008).
12. Angelskii O.V., Ushenko A.G., Arkhelyuk A.D., Yermolenko S.B., Burkovets D.N., Ushenko Yu.A. *Opt. Spektrosk*., **89**, 1050 (2000) [*Opt. Spectrosc*., **98**, 973 (2000)].
13. Angelsky O.V., Gorsky M.P., Maksimyak P.P., Maksimyak A.P., Hanson S.G., Zenkova C.Yu. *Opt. Express*, **19**, 660 (2011).
14. Angelsky O.V., Hanson S.G., Zenkova C.Yu., Gorsky M.P., Gorodyns'ka N.V. *Opt. Express*, **17**, 15623 (2009).
15. Makita S., Yasuno Y., Endo T., Itoh M., Yatagai T. *Opt. Review*, **12**, 146 (2005).
16. Makita S., Yasuno Y., Endo T., Itoh M., Yatagai T. *Appl. Opt*., **45**, 1142 (2006).
17. Pierce M.C., Strasswimmer J., Park B.H., Cense B., de Boer J.F. *J. Biomed. Opt*., **9**, 287 (2004).
18. Yasuno Y., Makita S., Sutoh Y., Itoh M., Yatagai T. *Opt. Lett*., **27**, 1803 (2002).
19. Pan Y., Li Z., Xie T., Chu C.R. *J. Biomed. Opt*., **8**, 648 (2003).
20. Ushenko A.G. *Opt. Spektrosk*., **91**, 340 (2001) [*Opt. Spectros*c., **91**, 313 (2001)].
21. Gori F., Santarsiero M., Vicalvi S., Borghi R., Guattari G. *Pure Appl. Opt*., **7**, 941 (1998).
22. Wolf E. *Phys. Lett. A*, **312**, 263 (2003).
23. Tervo J., Setala T., Friberg A. *Opt. Express*, **11**, 1137 (2003).
24. Ellis J., Dogariu A. *Opt. Lett*., **29**, 536 (2004).
25. Ushenko Y.O., Tomka Y.Y., Misevitch I.Z., Istratiy V.V., Telenga O.I. *Opt. Eng*., **50**, 039001 (2011).
26. Ushenko A.G., Tomka Yu.Yu., Dubolazov A.V. *Opt. Spektrosk*., **110**, 865 (2011) [*Opt. Spectrosc*., **110**, 814 (2011)].
27. Angelsky O.V., Ushenko A.G., Ushenko Y.G. *J. Biomed. Opt*., **10**, 060502 (2005).
28. Ushenko Y.A. *J. Biomed. Opt*., **16**, 066006 (2011).
29. Gerrard A., Burch J.M. *Introduction to Matrix Methods in Optics* (New York.: Wiley-Interscience Publ., 1975).
30. Angelskii O.V., Ushenko A.G., Arkhelyuk A.D., Yermolenko S.B., Burkovets D.N. *Opt. Spektrosk*., **88**, 495 (2000).
31. Ushenko A.G. *Opt. Spektrosk*., **89**, 601 (2000) [*Opt. Spectrosc*., **89**, 597 (2000)].
32. Pishak V., Ushenko A., Gryhoryshyn P., Yermolenko S., Rudeychuk V., Pishak O. *Proc. SPIE Int. Soc. Opt. Eng.*, **3317**, 418 (1997).
33. Angelsky O.V., Ushenko A.G., Ushenko Y.G., Tomka Y.Y. *J. Biomed. Opt*., **11**, 054030 (2006).
34. Angelsky O.V., Ushenko A.G., Ushenko Yu.A., Ushenko Ye.G. *J. Phys. D: Appl. Phys*., **39**, 3547 (2006).
35. Ushenko A.G. *Opt. Spektrosk*., **91**, 997 (2001) [*Opt. Spectrosc*., **91**, 932 (2001)].
36. Ushenko A.G. *Opt. Spektrosk*., **91**, 992 (2001) [*Opt. Spectrosc.*, **91**, 927 (2001)].
37. Dmitrieva O.A., Pigolkin Yu.I., Fedchenko T.M. *Sudebno-meditsinskaya ekspertiza polovykh funktsiy muzhchin* (Forensic Medical Examination of Male Sexual Function) (Vladivostok: LAINS, 2003) pp 18–20.
38. Frank G.A. *Prakticheskaya onkologiya*, **9** (2), 65 (2008).